

Atomic scale analysis of the GaP/Si(100) heterointerface by *in situ* reflection anisotropy spectroscopy and *ab initio* density functional theory

Oliver Supplie,^{1,2,3,*} Sebastian Brückner,^{1,2} Oleksandr Romanyuk,⁴ Henning Döscher,^{1,†} Christian Höhn,² Matthias M. May,^{2,3} Peter Kleinschmidt,^{1,2} Frank Grosse,⁵ and Thomas Hannappel^{1,2}

¹Technische Universität Ilmenau, Institut für Physik, Gustav-Kirchhoff-Straße 5, 98684 Ilmenau, Germany

²Helmholtz-Zentrum Berlin, Institute for Solar Fuels, Hahn-Meitner-Platz 1, 14109 Berlin, Germany

³Humboldt-Universität zu Berlin, Institut für Physik, Newtonstraße 15, 12489 Berlin, Germany

⁴Institute of Physics, Academy of Sciences of the Czech Republic, Cukrovarnická 10, 162 00 Prague 6, Czech Republic

⁵Paul-Drude-Institut für Festkörperelektronik, Hausvogteiplatz 5-7, 10117 Berlin, Germany

(Received 8 August 2014; revised manuscript received 31 October 2014; published 1 December 2014)

A microscopic understanding of the formation of polar-on-nonpolar interfaces is a prerequisite for well-defined heteroepitaxial preparation of III-V compounds on (100) silicon for next-generation high-performance devices. Energetically and kinetically driven Si(100) step formations result in majority domains of monohydride-terminated Si dimers oriented either parallel or perpendicular to the step edges. Here, the intentional variation of the Si(100) surface reconstruction controls the sublattice orientation of the heteroepitaxial GaP film, as observed by *in situ* reflection anisotropy spectroscopy (RAS) in chemical vapor ambient and confirmed by benchmarking to surface science analytics in ultrahigh vacuum. *Ab initio* density functional calculations of both abrupt and compensated interfaces are carried out. For P-rich chemical potentials at abrupt interfaces, Si-P bonds are energetically favored over Si-Ga bonds, in agreement with *in situ* RAS experiments. The energetically most favorable interface is compensated with an intermixed interfacial layer. *In situ* RAS reveals that the GaP sublattice orientation depends on the P chemical potential during nucleation, which agrees with a kinetically limited formation of abrupt interfaces.

DOI: [10.1103/PhysRevB.90.235301](https://doi.org/10.1103/PhysRevB.90.235301)

PACS number(s): 31.10.+z, 81.15.Gh, 68.35.Dv, 68.55.ag

I. INTRODUCTION

The combination of the outstanding optoelectronic properties of many III-V semiconductors with mature silicon-based microelectronics is greatly desired for next-generation high-performance devices [1,2]. Regarding solar-hydrogen generation for energy storage and renewable-fuel production, tandem structures reach optimum theoretical solar-to-hydrogen efficiencies applying Si as substrate and 1.6 to 1.8 eV band-gap absorbers [3]. The latter could be lattice-matched grown by dilute nitride Ga(N,As)P with theoretical photovoltaic tandem efficiencies close to optimum [4]. GaP-related surfaces and their interfaces to water are the subject of current theoretical [5–7] as well as experimental [8] studies, and the combination with Si(100) for photoelectrochemical (PEC) diodes is highly desired for water splitting [9]. Pseudomorphic GaP/Si(100) serves as a quasisubstrate for the subsequent industrially scalable growth of high-performance electronic and optoelectronic devices, such as multijunction solar cells [4,10] or PEC diodes, by metal-organic vapor phase epitaxy (MOVPE). However, an understanding of the formation of the heterointerface at the atomic scale is desired to achieve integration of III-V semiconductors on Si(100) with low-defect densities.

Single-layer substrate steps at a III-V/IV(100) heterointerface, for example, inherently induce antiphase disorder in the III-V film [11,12]. Antiphase boundaries (APBs), which separate antiphase domains (APDs), are characterized by homopolar bonds which act as recombination centers degrading

device efficiency. In contrast, double-layer (or even-numbered) steps at the substrate surface prior to heteroepitaxy enable APD-free III-V growth. Double-layer steps at a dimerized Si(100) surface coincide with identically oriented dimers on adjacent terraces [13] due to the tetrahedral coordination within the diamond lattice. Dimers oriented perpendicular to the step edges (i.e., dimer rows parallel to the step edges) form so-called A-type or (1×2) reconstructed terraces, while dimers oriented parallel to the step edges (i.e., dimer rows perpendicular to the step edges) form so-called B-type or (2×1) reconstructed terraces [13]. Preferentially double-layer stepped, monohydride-terminated Si(100) surfaces with different misorientations have recently been prepared under *in situ* control with reflection anisotropy spectroscopy (RAS) in vapor-phase epitaxy (VPE) ambient [14–16]. While predicted to be energetically unfavorable [17–19], stable A-type terraces form on Si(100) with 2° misorientation towards the [011] direction (in the following, called Si(100) $2^\circ \rightarrow$ [011]) during a well-defined preparation in hydrogen [15]. Layer-by-layer removal, however, leads to an oscillation of the predominant domain on low-offcut Si(100) surfaces [16].

GaP/Si(100) is the appropriate material system to study subsequent polar-on-nonpolar heteroepitaxy since gallium phosphide is almost lattice matched to silicon. Recently, the atomic structure of the GaP/Si(100) interface was investigated *ex situ* by transmission electron microscopy (TEM) and simplified abrupt interface structure models with either Si-Ga or Si-P interface bonds were proposed [20]. According to these models, Si-Ga bonds were formed during a pulsed nucleation starting with the P precursor at around 400 °C, while Si-P bonds were formed at elevated temperatures for the very first pulse. Silicon preparation in hydrogen ambient, however, is a highly nonequilibrium process, in particular

*oliver.supplie@tu-ilmenau.de

†Present address: National Renewable Energy Laboratory, 15013 Denver West Parkway, Golden, Colorado 80401, USA.

for low misorientations at elevated temperatures [16], and *in situ* monitoring is indispensable. Reflection anisotropy spectroscopy has been established as a surface-sensitive *in situ* optical probe of cubic crystals in vapor-phase ambient [21,22]. Dimerized (100) surface reconstructions of cubic crystals often exhibit characteristic reflection anisotropy (RA) spectra [23], as reported for both monohydride-terminated Si(100) [14–16,24] and for P-rich GaP(100) [25,26]. By definition, identical anisotropic structures with mutually perpendicular orientation exhibit RA spectra with opposite signs. In consequence, RAS enables *in situ* quantification of the domain content at dimerized surfaces [27,28].

Atomic structures of heterointerfaces of zinc-blende and wurtzite semiconductor superlattices were investigated in detail by *ab initio* density functional theory (DFT) calculations [29–33]. Heterovalent bonding configurations at abrupt (100) interfaces were found to be energetically unfavorable in comparison to compensated interfaces, where atomic intermixture across the interface satisfies the electron-counting rule model (ECM). Charge compensation at the interface can be realized by atomic intermixture within a single interfacial layer [34]. For GaP/Si(111) heterostructures, however, the thermodynamically stable GaP(111)A/Si(111) heterointerface was found to be uncompensated and abrupt under P-rich conditions, while it is compensated under Ga-rich conditions. The GaP(111)B/Si(111) interface was found to be compensated for both P-rich and Ga-rich conditions [35].

Here, we study the atomic interface structure of GaP/Si(100) heterointerfaces with *in situ* RAS and *ab initio* DFT calculations. We show that we can choose between energetically and kinetically driven step formation at Si(100) surfaces by varying the experimental conditions and thereby direct the majority dimer orientation. We investigate the influence of mutually perpendicular dimer orientations of the nonpolar Si(100) substrates on subsequent GaP nucleation and growth of polar GaP epilayers with *in situ* RAS. *Ab initio* DFT calculations are carried out to predict the energetically most favorable interface structures both for abrupt interfaces and interfaces with atomic intermixture in the interfacial layer. We show that RAS allows one to analyze the sublattice orientation of the GaP film with respect to the silicon substrate using *in situ* data only and, in combination with the theoretical results, we suggest possible interface models for the GaP/Si(100) heterostructures.

II. EXPERIMENT

Samples were prepared by MOVPE (Aixtron AIX-200) under Pd-purified H₂ flow. Temperatures were measured with a thermocouple inside the susceptor. *n*-type doped Si(100) substrates with 2° miscut towards the [011] direction were thermally deoxidized (950 mbar, 1000 °C, 30 min, without additional wet-chemical pretreatment), a 0.25- μ m-thick silicon buffer was grown using silane (200 mbar, 1000 °C) and annealed (950 mbar, 1000 °C, 10 min). Dependent on the intended surface reconstruction of the Si(100) substrate, we varied the subsequent preparation: (i) annealing at 1000 °C and 50 mbar and fast cooling for the monohydride-terminated surface with preferential B-type domains, and (ii) annealing at 730 °C (950 mbar) before cooling for the monohydride-

terminated surface with A-type majority domains. On both A-type and B-type substrates, GaP was nucleated with tertiary-butylphosphine (TBP, C₄H₁₁P) and triethylgallium (TEGa, C₆H₁₅Ga) pulses at 420 °C and 100 mbar (starting with TBP) and grown for 70 s at 595 °C. The P-rich GaP surfaces were prepared by annealing without TBP at 420 °C [28]. We monitored the entire MOVPE process with RAS (LayTec EpiRAS 200). RAS measures the normalized difference in reflection of linearly polarized light along two mutually perpendicular crystal axes, aligned here such that

$$\frac{\Delta r}{r} = 2 \frac{r_{[0\bar{1}1]} - r_{[011]}}{r_{[0\bar{1}1]} + r_{[011]}}, \quad (1)$$

where r is the complex amplitude reflection coefficient. The amplitudes of the spectra were corrected regarding a Si(110) reference, and a baseline accounting for contributions of the optical setup was subtracted. Our MOVPE reactor is connected to a vacuum chamber allowing contamination-free transfer [36] from MOVPE ambient to ultrahigh vacuum (UHV), so that x-ray photoelectron spectroscopy (XPS, Specs Focus 500 and Phoibos 100), scanning tunneling microscopy (STM) (SPECS 150 Aarhus), and low-energy electron diffraction (LEED, Specs ErLEED 100-A) were accessible via a mobile UHV shuttle [36].

III. COMPUTATIONS

The *ab initio* calculations of relative interface formation energies were carried out using the ABINIT program [37,38]. The generalized gradient approximation (GGA) for the exchange-correlation energy functional was used. Norm-conserving pseudopotentials [39] of the Troullier-Martins type [40] were used to describe the atomic species. The electronic wave functions were expanded in a plane-wave basis with a converged kinetic-energy cutoff of 12 Hartree (Ha). k point sets [41] corresponding to 12 \times 12 points per (1 \times 1) Brillouin zone were used. Periodic boundary conditions were applied along the in-plane and out-of-plane directions. A slab consisted of 5 bilayers of GaP and 10 layers of Si. The surface was terminated by the (2 \times 2) surface reconstruction consisting of two P dimers and two hydrogen atoms per (2 \times 2) surface cell [26]. The surface reconstruction does obey the ECM [42]. Dangling bonds of the Si layer back side were passivated by hydrogen atoms. A vacuum region of 20 Å was used to avoid surface interaction with the bottom layer.

Equilibrium lattice constants were computed for bulk Si ($a_{\text{Si}} = 5.46$ Å) and GaP ($a_{\text{GaP}} = 5.50$ Å) [35]. The Si lattice constant was used for the GaP/Si slab. The atomic positions were adjusted until the interatomic forces became smaller than 10⁻³ Ha/Bohr, whereas atomic positions of two Si layers and passivating hydrogen atoms were fixed. The relative interface formation energy $\Delta\gamma$, as a function of the chemical potential variation in thermodynamic equilibrium, is defined as [32,33]

$$\Delta\gamma \mathcal{A} = E_{\text{tot}} - (n_{\text{P}} - n_{\text{Ga}})\Delta\mu_{\text{P}} - n_{\text{Ga}}\mu_{\text{GaP}}^{\text{bulk}} - n_{\text{Si}}\mu_{\text{Si}}^{\text{bulk}},$$

where E_{tot} is the total energy of the slab, n_{P} , n_{Ga} , n_{Si} are the number of P, Ga, and Si atoms in a slab, respectively, μ_i is a chemical potential of species i , $\Delta\mu_{\text{P}} = \mu_{\text{P}} - \mu_{\text{P}}^{\text{bulk}}$, and \mathcal{A} is the surface unit cell area. The boundary conditions for the

chemical potential variation are expressed as

$$H_f^{\text{GaP}} \leq \Delta\mu_P \leq 0,$$

where H_f^{GaP} is the heat of formation of GaP. The corresponding bulk chemical potentials were calculated for the orthorhombic α -Ga phase [43] and the orthorhombic black P [44] phase. The computed value of the GaP heat of formation is $H_f^{\text{GaP}} = -0.91$ eV [45].

IV. RESULTS AND DISCUSSION

A. *In situ* RAS of Si(100) and GaP/Si(100) surfaces

Figure 1 shows the *in situ* RAS signals of the two differently prepared Si(100) substrates prior to III-V nucleation and their benchmarking by low-energy electron diffraction (LEED) and scanning tunneling microscopy (STM). While the line shapes of both RA spectra are similar, sign and amplitude of the signals differ. The green line in Fig. 1(a) depicts the RA spectrum of a monohydride-terminated Si(100) sample

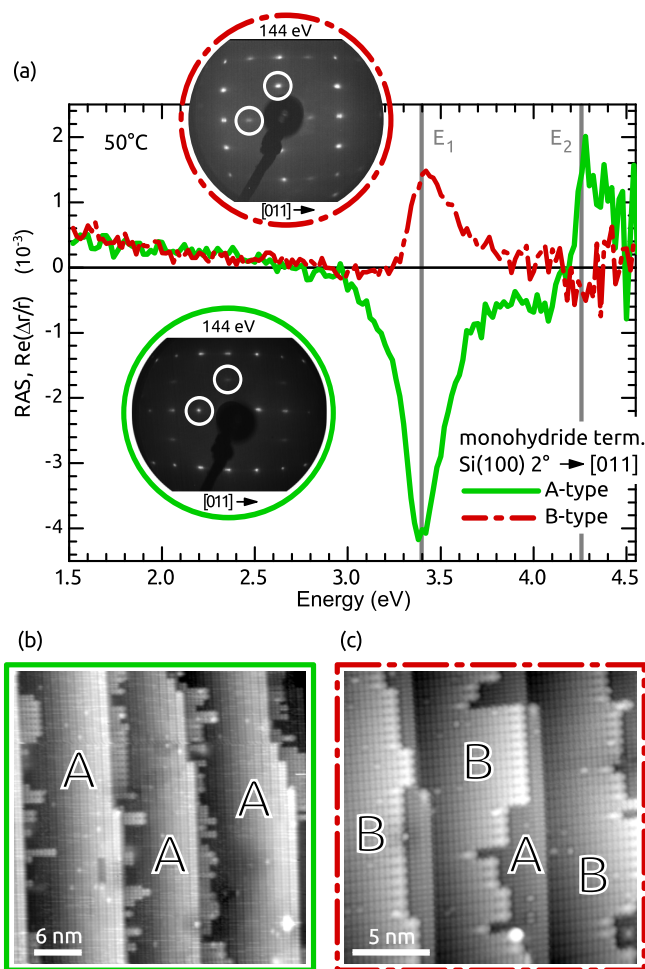


FIG. 1. (Color online) (a) RA spectra of monohydride-terminated Si(100) $2^\circ \rightarrow [011]$ with A-type majority domains (green line) and B-type majority domains (red broken line), respectively (both measured at 50°C). Vertical gray lines mark the critical point energies of Si [46]. Insets: LEED patterns of both samples; half-order spots occur (marked with white circles) along the dimer orientation of the majority domain. STM images (empty states) of the (b) A-type and (c) B-type sample where letters denote the terrace type.

annealed at about 730°C in 950 mbar H_2 , as shown in Ref. [15] and abbreviated as Si-A in the following. Characteristic features are a pronounced local minimum at E_1 , a shoulder between 3.6 and 4.0 eV, and a local maximum at the E_2 critical point energy [15,27]. The corresponding STM image [Fig. 1(b)], measured after contamination-free transfer to UHV [36], shows mainly A-type terraces with dimer rows oriented parallel to the step edges along the $[0\bar{1}1]$ direction. Only small residuals of B-type terraces are visible, which indicates an almost single-domain surface. Accordingly, the half-order diffraction spots in the corresponding LEED pattern [Fig. 1(a), green framed inset] are intense along the $[011]$ direction.

Annealing at about 950°C in 50 mbar H_2 and fast cooling leads to an RA spectrum of flipped sign [Fig. 1(a), broken red line], but with similar line shape. Both sign and line shape agree with theoretical predictions, which Palumbo *et al.* [27] performed for the RA spectrum of monohydride-terminated B-type Si(100), as well as with the RA spectra presented by Shioda and van der Weide for surface preparation in UHV [24]. The corresponding STM image in Fig. 1(c) shows a prevalence of dimer rows perpendicular to the step edges (B-type domains) and smaller A-type domains on subjacent terraces (marked B and A, respectively). The associated LEED pattern [inset in Fig. 1(a)] shows enhanced intensity of the spots at half order along the $[0\bar{1}1]$ direction compared to the $[011]$ direction, indicating (2×1) majority domains. RAS inherently integrates over the probed area (at mm^2 scale) so that both types of domains contribute to the spectrum, and the RAS amplitude, consequently, is a measure for the domain ratio [27,28]. The amplitude of the dashed-red RA spectrum in Fig. 1(a) corresponds to a B-type:A-type domain concentration ratio of about 62:38 [27]. The B-type monohydride-terminated Si(100) surface will be denoted Si-B in the following. A crucial step in the preparation of Si-B in hydrogen ambient is fast cooling at low pressures in order to avoid the formation of preferential A-type domains [15] due to Si atom removal in H_2 . A cooling ramp at pressures below 50 mbar might increase the domain ratio further towards the B type.

The Si(100) surface preparation is either governed by kinetics [15] (as discussed for the “anomalous” A-type surface [15]) or energetics (for the B-type surface) so that the choice of the process parameters allows one to direct the majority dimer orientation as intended for subsequent processing. The presented RA spectra in Fig. 1(a) thereby enable *in situ* identification of Si(100) $2^\circ \rightarrow [011]$ surfaces with both A-type and B-type majority domains, which is of the utmost importance directly before III-V nucleation.

The impact of the majority domains at the Si(100) substrate on subsequent GaP heteroepitaxy will be discussed in the following. Both P-rich GaP(100) [25] and P-rich GaP/Si(100) surfaces [28] prepared in H_2 ambient exhibit $(2 \times 2)/c(4 \times 2)$ reconstructions formed by buckled P dimers with one H atom per dimer. The resulting dielectric anisotropies at the surface give rise to characteristic RA spectra [25,26]. We applied identical GaP nucleation and growth processes on both Si-A and Si-B substrate surfaces (as confirmed by *in situ* RAS directly before nucleation; cf. Fig. 1). The resulting RA spectra of the P-rich GaP/Si(100) surfaces are shown in Fig. 2(a).

RA spectra of P-rich GaP/Si(100) are well known in literature [28]. Figure 2(c) shows the LEED pattern of such

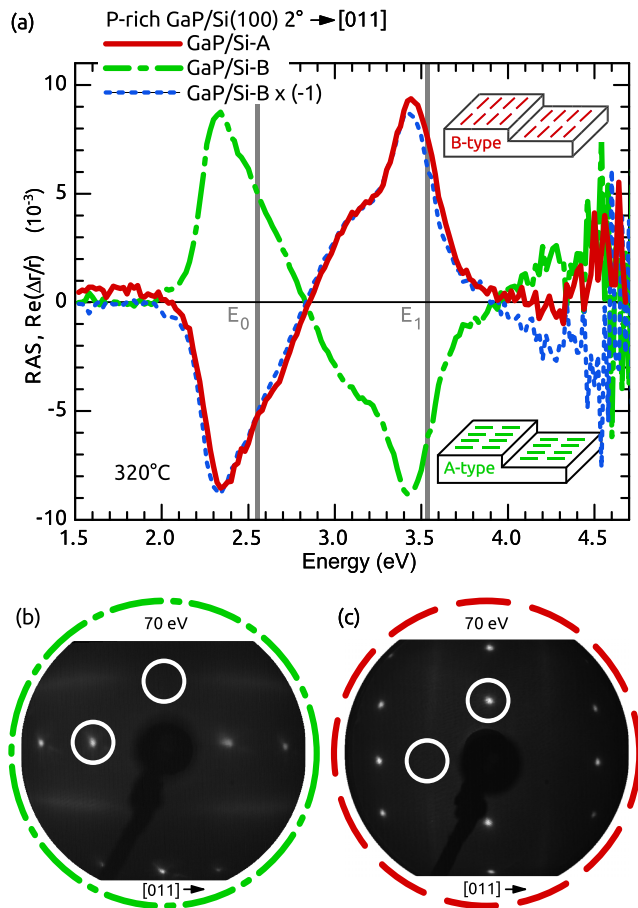


FIG. 2. (Color online) RA spectra of about 40-nm-thin GaP films grown on Si-A (red line) and Si-B (broken green line) surfaces, as well as the latter spectrum flipped in sign (dotted blue line) for comparison. The line color corresponds to the P-dimer orientation, while the line style indicates on which substrate GaP was grown [in reference to Fig. 1(a)]. Insets: The corresponding P-dimer orientation of the majority domain at the P-rich GaP/Si(100) surface. Vertical gray lines mark critical point energies of GaP [47]. LEED patterns of the (b) GaP/Si-B sample and of a (c) $(2 \times 2)/c(4 \times 2)$ reconstructed GaP(100) reference sample.

a P-rich GaP(100) reference surface with a $(2 \times 2)/c(4 \times 2)$ reconstruction where the P dimers are aligned (2×1) -like (B type), leading to half-order spots along the $[0\bar{1}1]$ direction. Note that the notation of A-type and B-type here refers to the P-dimer orientation at the surface according to Chadi [13], which is opposite to the notation of A- and B-type “polarity” for P-rich GaP(100). The RAS signal of the heteroepitaxial GaP/Si-A sample (Fig. 2, red line) is very similar to that of P-rich GaP(100) [25] regarding both line shape and, particularly, sign of the signal: The sign of the surface-state related peak at about 2.35 eV and the peak at about 3.4 eV clearly corresponds to a B-type $(2 \times 2)/c(4 \times 2)$ reconstructed P-rich GaP/Si(100) surface as known for P-rich GaP(100) [25,26]. Modulations of the amplitude of the signal are related to internal reflection of the incoming light at the heterointerface [28,48].

Identical GaP growth conditions applied on a Si-B substrate result in an RAS signal of opposite sign (Fig. 2, broken green line). Since a flipped sign in the RAS signal implies a mutually perpendicular anisotropic structure giving rise to the spectral

TABLE I. Principally possible substrate/film orientations starting with either Ga or P at an abrupt heterointerface. Note that all samples were prepared P rich with P dimers at the surface.

Substrate	GaP epilayers	Orientation	Case
Si-A	Ga-P-[...]-Ga-P	A-type	A \rightarrow A
Si-A	P-Ga-[...]-P	B-type	A \rightarrow B
Si-B	Ga-P-[...]-Ga-P	B-type	B \rightarrow B
Si-B	P-Ga-[...]-P	A-type	B \rightarrow A

features, this corresponds to a $(2 \times 2)/c(4 \times 2)$ reconstruction of the GaP/Si-B surface where the P dimers are aligned (1×2) -like (A type), as also evidenced in the LEED pattern of the sample [Fig. 2(b)]. When flipped in sign (Fig. 2, dotted blue line), the RAS signal of GaP/Si-B is almost identical with that of GaP/Si-A up to about 4 eV. The amplitude of both signals indicates almost single-domain surfaces, implying self-annihilation [49] of antiphase boundaries during GaP growth on Si-B. The orientation of the P dimers at the GaP/Si(100) interface thus depends on that of the Si(100) substrate. Due to the tetrahedral coordination of atoms within the zinc-blende lattice, the dimer orientation on the P-rich GaP/Si(100) surface reflects the GaP sublattice orientation. We can thus choose the intended sublattice orientation for further processing [50] via the substrate preparation.

B. Experimentally observed GaP/Si(100) interface structures

The GaP sublattice orientation, which we determined by the orientation of P dimers at the GaP/Si(100) surface, is correlated with the heterointerface structure between the Si substrate and the GaP film: Considering the prevalent dimer orientation of Si-A and Si-B substrates and the tetrahedral coordination in the crystal lattice, an inverted sublattice in the GaP film would result depending on whether bonds between Si and Ga or Si and P are preferred for both Si-A and Si-B. Table I displays all possible substrate/film orientations for abrupt heterointerfaces. Si-Ga interfaces at Si-A (Si-B) substrates would lead to A-type (B-type) P dimers at the GaP/Si(100) surface, while Si-P interfaces at Si-A (Si-B) substrates correspond to B-type (A-type) P dimers at the GaP/Si(100) surface.

First, we will assume the abrupt interface, which is also discussed by Beyer *et al.* [20]. While this configuration is not the energetically most favored one, growth in MOVPE, however, takes place under highly nonequilibrium conditions and even energetically less favored states may result and be “frozen” in the following process (cf. the kinetically driven A-type Si(100) preparation [15] discussed above). As obvious from Figs. 1 and 2, we observed the cases A \rightarrow B and B \rightarrow A (Table I) in our experiments. Following an idealized abrupt interface model [20], Figs. 3(a) and 3(b) show that our experiments suggest Si-P interfaces both for Si-A and Si-B. In contrast, Beyer *et al.* [20] reported that Si-Ga bonds are created on Si(001) with 0.1° misorientation towards the $[110]$ direction and A-type majority domains during a pulsed GaP nucleation, while the growth of inverted GaP required a modified nucleation with a higher temperature (about 680°C) during the first TBP pulse, which was attributed to TBP decomposition [20]. Particularly in this temperature range,

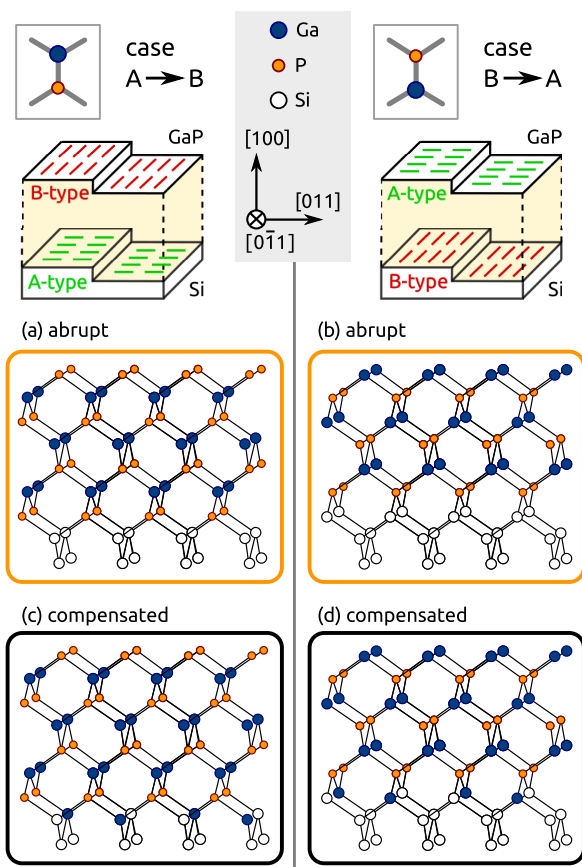


FIG. 3. (Color online) Abrupt interface model (in side view) for the experimentally observed cases A → B (left) and B → A (right). The sketch in the upper part indicates the dimer orientations of the Si(100) substrate prior to GaP nucleation and of the final P-rich GaP/Si(100) surface as obtained by *in situ* RAS (cf. Figs. 1 and 2). Inset: The corresponding sublattice orientation of the GaP film. In an idealized abrupt interface model, both (a) B-type GaP grown on Si-A and (b) A-type GaP grown on Si-B require Si-P bonds at the heterointerface. (c), (d) Visualization of the binding situation at compensated 0.5 Si : 0.5 Ga-P interfaces.

however, *in situ* control is of utmost importance regarding almost nominal Si(100) substrates where the majority domain changes periodically from A type to B type due to layer-by-layer removal in H_2 process ambient [16]. The Si(100) $2^\circ \rightarrow [011]$ substrates used for this study form stable A-type or B-type terraces depending on the annealing procedure (see above) as confirmed *in situ* by RAS. Wright *et al.* [51] reported for GaP nucleation on Si(211) that P binds to Si atoms having two back bonds and that P might even displace Ga atoms occupying such sites due to the weaker Si-Ga bond strength. Considering that the Si dimers at the substrate will break during nucleation, this agrees with a prevalence of Si-P bonds at the GaP/Si(100) heterointerface and such group-IV–group-V bonds at the heterointerface similarly occur for GaAs growth on both Si(100) [52] and Ge(100) [53]. Bringans [54] even argues that in earlier GaAs/Si(100) studies applying Ga prelayer deposition before actual growth, the Ga atoms may have been displaced by As atoms.

Since a P (Ga) atom has five (three) valence electrons, which is $5/4$ ($3/4$) partial electronic charge per bond, and

two electrons are required for each bond, there is $1/4$ excess (deficit) of electronic charge per (1×1) interface cell formed by a Si-P (Si-Ga) bond at abrupt interfaces. Such a heterovalent GaP/Si(100) interface can be compensated by Si/Ga (Si/P) atomic intermixture during the initial stage of growth. For other semiconductor heterostructures, it was found that atomic intermixture at the interface leads to a lower interface formation energy compared to abrupt interfaces [29–33]. Atomic intermixture within the interface layer is associated with an electron charge redistribution among the (III-V)–IV bonds so that the ECM [42] is fulfilled within the interface. Recently, GaP/Si(111) heterointerface structures were investigated by *ab initio* DFT calculations. It was found that the interface energy decreases for the majority of charge compensated interfaces with Si/P (Si/Ga) atomic intermixture in the interfacial layer, with the exception of the P-rich GaP(111)/Si(111) interface [35]. The smallest in-plane interface unit cell where charge can be compensated is a (2×1) cell with a Si to P (Ga) atomic mixing ratio of 0.5:0.5. A mixed heterointerface structure model for GaP/Si(100), where every second Si atom is substituted by a Ga atom at the interface (0.5 Si : 0.5 Ga-P model), would also agree with the observed cases A → B and B → A, as shown in Figs. 3(c) and 3(d). In the following section, we will calculate interface formation energies of both abrupt and compensated GaP/Si(100) interface structures.

C. *Ab initio* DFT calculations

Ab initio DFT calculations were carried out for $T = 0$ K assuming thermodynamic equilibrium during initial stages of interface formation. These equilibrium interface structures can be regarded as reference points, even though real atomic interface arrangements can deviate, for example due to kinetically limiting and nonequilibrium growth processes, hydrogen interaction at elevated temperatures, etc. For the DFT calculations of the relative interface formation energies $\Delta\gamma$ of abrupt Si-Ga, Si-P, and compensated 0.5 Si : 0.5 P-Ga, 0.5 Si : 0.5 Ga-P interface structure models, we fixed the surface structure to the P-terminated (2×2) reconstruction for both sublattice orientations of the GaP film and varied the atomic stoichiometry at the interface: The Si-P (Si-Ga) abrupt interface consists of four Si and four P (Ga) atoms per (2×2) in-plane cell [see Fig. 4(a)]. A compensated Si-P (Ga) interface is formed when two Si atoms are substituted by two Ga (P) atoms per (2×2) cell with a Si:P (Ga) ratio of 0.5:0.5 within the interfacial layer [see Fig. 4(b)]. Figure 4(c) shows the resulting dependence of $\Delta\gamma$ on the P chemical potential. The compensated interface structure with a 0.5 Si : 0.5 Ga-P atomic interfacial layer is found to be the energetically most favorable in thermodynamic equilibrium. Atomic intermixture of Si and P at the interface is found to be energetically less favorable. Similar to other semiconductor heterostructures, abrupt interfaces were found to be energetically less stable in equilibrium than the compensated interfaces. Abrupt Si-P and Si-Ga interfaces, however, could be realized under nonequilibrium growth conditions, such as MOVPE preparation. The formation energy of the abrupt interfaces depends on the chemical potential: for P-rich conditions (which are typical during MOVPE preparation), Si-P bonds are favored and $\Delta\gamma$ increases linearly with decreasing P chemical potential. From

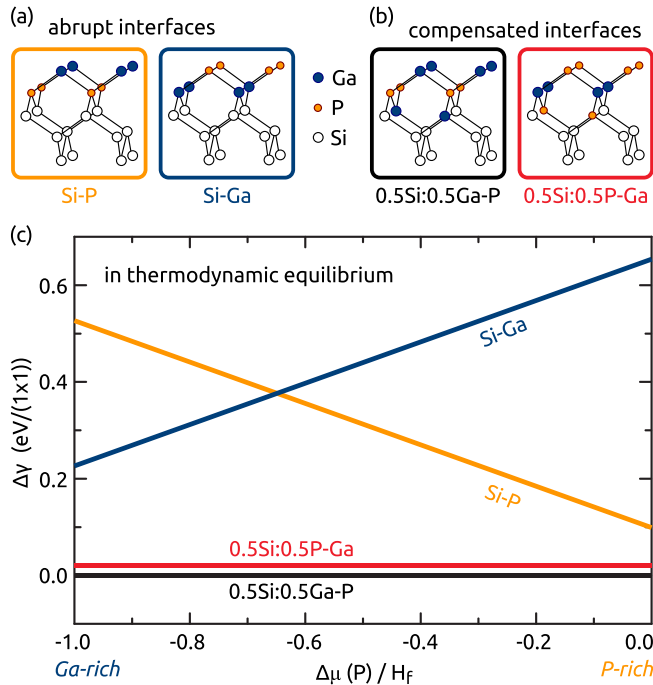


FIG. 4. (Color online) Structural models for (a) abrupt and (b) compensated GaP/Si(100) interfaces. (c) Relative interface formation energy diagram of these heterostructures. The interface energy of the 0.5 Si : 0.5 Ga-P structure, which is the most stable configuration at thermodynamic equilibrium, was used as reference energy and was set to zero.

a certain threshold value towards Ga-rich conditions, Si-Ga bonds are lower in energy. The energy of the Si-P interface is much lower at P-rich conditions than the energy of the Si-Ga interface under Ga-rich conditions. This result is in agreement with the previous theoretical work on the abrupt GaP/Si(100) interface [55] predicting a higher stability of Si-P bonds compared to Si-Ga bonds, which agrees with earlier experimental results regarding thermal stability [56].

In order to find experimental indications as to whether the abrupt Si-P or the compensated 0.5 Si : 0.5 Ga-P interface model is more suitable to describe our results from Fig. 3, we intentionally varied the chemical potential.

D. Variation of the chemical potential

Precursor residuals and coated surfaces in the MOVPE reactor result in a background pressure which can be controlled in a certain range and allows one to vary the chemical potential. Since quick pressure ramps after Si buffer growth increase diffusion on the surface prior to nucleation, we performed these experiments on Si(100) $0.1^\circ \rightarrow [011]$ to be able to prepare A-type substrate surfaces [16]. We could vary the Ga:P ratio on the surface prior to nucleation from about 0.1 to 2.5, as confirmed by x-ray photoelectron spectroscopy after Si preparation (with increasing amount of Ga and almost constant amount of P, not shown here). Figure 5 shows the RA spectra of P-rich GaP/Si(100) $0.1^\circ \rightarrow [011]$ for a sample prepared in “P-rich” (orange line) and more “Ga-rich” (blue line) reactor conditions. Prior to nucleation, the sign of the RA spectra of both Si(100) substrates corresponded to A-

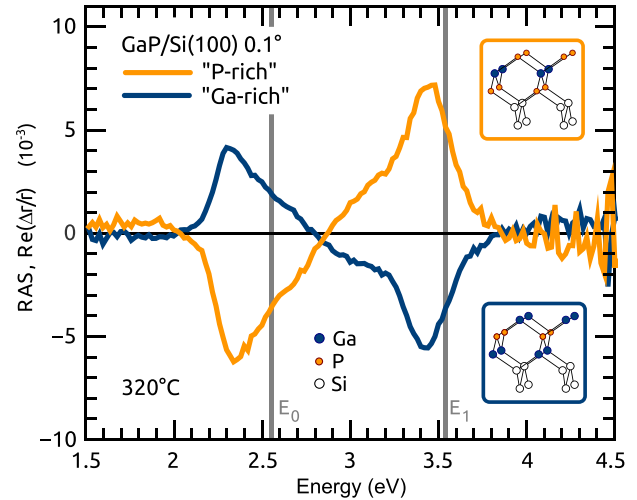


FIG. 5. (Color online) RA spectra of about 40-nm-thin GaP films grown on Si(100) $0.1^\circ \rightarrow [011]$ prepared in different reactor conditions. With increasing amount of Ga at the surface, the P-dimer orientation changes from B type (orange line) to A type (blue line). Insets: The corresponding interface structure in the case of abrupt interfaces. Vertical gray lines mark critical point energies of GaP [47].

type majority domains. We conclude that case A \rightarrow A (Table I, corresponding to Si-Ga bonds if abrupt interfaces are assumed) occurs in Ga-rich reactor conditions, which could also explain the findings in Ref. [20], while case A \rightarrow B is realized under P-rich conditions. Accordingly, the GaP sublattice orientation and thus the binding situation at the GaP/Si(100) interface depends on the chemical potential. This is not the case for the compensated interfaces predicted by the theory (Fig. 4). Consequently, the combination of our theoretical and experimental results suggests a kinetically limited formation of abrupt GaP/Si(100) heterointerfaces. This does not, however, completely exclude diffusion of individual atoms.

V. CONCLUSION

We prepare and analyze both preferential A-type and B-type Si(100) surfaces in H_2 ambient depending on thermodynamic state functions (T , p_{H_2}), leading to a surface formation governed either by kinetics or energetics. The directions of the majority dimers are monitored with optical *in situ* spectroscopy (RAS). Applying identical GaP nucleation, we prepare B-type GaP on monohydride-terminated, A-type Si(100), while A-type GaP grows on monohydride-terminated, B-type Si(100). The correlation between dimer orientations (i) at Si(100) directly prior to nucleation and (ii) at the P-rich GaP/Si(100) surface indicates that Si-P bonds are favored during the formation of the crucial heterointerface when applying an abrupt interface model. Also, *ab initio* DFT calculations favor abrupt Si-P over abrupt Si-Ga interfaces for a wide range of chemical potentials. The DFT calculations reveal that the energetically more favored heterointerface structure in equilibrium consists of Si/Ga atomic intermixture with a ratio of 0.5/0.5. However, RAS experiments display a dependence of the GaP sublattice orientation on the chemical potential during nucleation, in agreement with the kinetically limited, abrupt GaP/Si(100) interface model.

ACKNOWLEDGMENTS

This work was financially supported by the BMBF (Project No. 03SF0404A) and Deutsche Forschungsgemeinschaft (DFG) (Project No. HA3096). O.R. acknowledges support by ASCR (Project No. M100101201). H.D. appreciates

financial support by a EU Marie Curie fellowship (IOF No. 300971). M.M.M. gratefully acknowledges support of a Ph.D. scholarship of the Studienstiftung des deutschen Volkes e.V. The authors highly appreciate J. Luczaks' support during the STM measurements and would like to thank G. Steinbach and S. Gemming for fruitful discussions.

-
- [1] J. A. del Alamo, *Nature (London)* **479**, 317 (2011).
 [2] R. F. Service, *Science* **323**, 1000 (2009).
 [3] S. Hu, C. Xiang, S. Haussener, A. D. Berger, and N. S. Lewis, *Energy Environ. Sci.* **6**, 2984 (2013).
 [4] H. Döscher, O. Supplie, M. M. May, P. Sippel, C. Heine, A. G. Muñoz, R. Eichberger, H.-J. Lewerenz, and T. Hannappel, *ChemPhysChem* **13**, 2899 (2012).
 [5] S. Jeon, H. Kim, W. A. Goddard, and H. A. Atwater, *J. Phys. Chem. C* **116**, 17604 (2012).
 [6] B. C. Wood, T. Ogitsu, and E. Schwegler, *J. Chem. Phys.* **136**, 064705 (2012).
 [7] B. C. Wood, E. Schwegler, W. I. Choi, and T. Ogitsu, *J. Phys. Chem. C* **118**, 1062 (2014).
 [8] M. M. May, O. Supplie, C. Höhn, R. van de Krol, H.-J. Lewerenz, and T. Hannappel, *New J. Phys.* **15**, 103003 (2013).
 [9] O. Supplie, M. M. May, H. Stange, C. Höhn, H.-J. Lewerenz, and T. Hannappel, *J. Appl. Phys.* **115**, 113509 (2014).
 [10] J. F. Geisz, J. M. Olson, D. J. Friedman, K. M. Jones, R. C. Reedy, and M. J. Romero, *IEEE Photovol. Spec. Conf.* **31**, 695 (2005).
 [11] H. Kroemer, *J. Cryst. Growth* **81**, 193 (1987).
 [12] S. F. Fang, K. Adomi, S. Iyer, H. Morkoc, H. Zabel, C. Choi, and N. Otsuka, *J. Appl. Phys.* **68**, R31 (1990).
 [13] D. J. Chadi, *Phys. Rev. Lett.* **59**, 1691 (1987).
 [14] H. Döscher, A. Dobrich, S. Brückner, P. Kleinschmidt, and T. Hannappel, *Appl. Phys. Lett.* **97**, 151905 (2010).
 [15] S. Brückner, H. Döscher, P. Kleinschmidt, O. Supplie, A. Dobrich, and T. Hannappel, *Phys. Rev. B* **86**, 195310 (2012).
 [16] S. Brückner, P. Kleinschmidt, O. Supplie, H. Döscher, and T. Hannappel, *New J. Phys.* **15**, 113049 (2013).
 [17] T. W. Poon, S. Yip, P. S. Ho, and F. F. Abraham, *Phys. Rev. Lett.* **65**, 2161 (1990).
 [18] F. A. Reboredo, S. B. Zhang, and A. Zunger, *Phys. Rev. B* **63**, 125316 (2001).
 [19] A. R. Laracuenta and L. J. Whitman, *Surf. Sci.* **545**, 70 (2003).
 [20] A. Beyer, J. Ohlmann, S. Liebich, H. Heim, G. Witte, W. Stolz, and K. Volz, *J. Appl. Phys.* **111**, 083534 (2012).
 [21] D. E. Aspnes and A. A. Studna, *Phys. Rev. Lett.* **54**, 1956 (1985).
 [22] P. Weightman, D. S. Martin, R. J. Cole, and T. Farrell, *Rep. Prog. Phys.* **68**, 1251 (2005).
 [23] J.-T. Zettler, *Prog. Cryst. Growth Ch.* **35**, 27 (1997).
 [24] R. Shioda and J. van der Weide, *Appl. Surf. Sci.* **130–132**, 266 (1998).
 [25] L. Töben, T. Hannappel, K. Möller, H. Crawack, C. Pettenkofer, and F. Willig, *Surf. Sci.* **494**, L755 (2001).
 [26] P. H. Hahn, W. G. Schmidt, F. Bechstedt, O. Pulci, and R. Del Sole, *Phys. Rev. B* **68**, 033311 (2003).
 [27] M. Palummo, N. Witkowski, O. Pluchery, R. Del Sole, and Y. Borenstein, *Phys. Rev. B* **79**, 035327 (2009).
 [28] H. Döscher and T. Hannappel, *J. Appl. Phys.* **107**, 123523 (2010).
 [29] D. B. Laks and A. Zunger, *Phys. Rev. B* **45**, 14177 (1992).
 [30] N. Chetty and R. M. Martin, *Phys. Rev. B* **45**, 6074 (1992).
 [31] N. Chetty and R. M. Martin, *Phys. Rev. B* **45**, 6089 (1992).
 [32] A. Kley and J. Neugebauer, *Phys. Rev. B* **50**, 8616 (1994).
 [33] J. Pezold and P. Bristowe, *J. Mater. Sci.* **40**, 3051 (2005).
 [34] N. Nakagawa, H. Y. Hwang, and D. A. Muller, *Nat. Mater.* **5**, 204 (2006).
 [35] O. Romanyuk, T. Hannappel, and F. Grosse, *Phys. Rev. B* **88**, 115312 (2013).
 [36] T. Hannappel, S. Visbeck, L. Töben, and F. Willig, *Rev. Sci. Instrum.* **75**, 1297 (2004).
 [37] X. Gonze, J.-M. Beuken, R. Caracas, F. Detraux, M. Fuchs, G.-M. Rignanese, L. Sindic, M. Verstraete, G. Zerah, F. Jollet, M. Torrent, A. Roy, M. Mikami, P. Ghosez, J.-Y. Raty, and D. Allan, *Comput. Mater. Sci.* **25**, 478 (2002).
 [38] X. Gonze, G.-M. Rignanese, M. Verstraete, J.-M. Beuken, Y. Pouillon, R. Caracas, F. Jollet, M. Torrent, G. Zerah, M. Mikami, P. Ghosez, M. Veithen, J.-Y. Raty, V. Olevano, F. Bruneval, L. Reining, R. Godby, G. Onida, D. R. Hamann, and D. C. Allan, *Z. Kristallogr.* **220**, 558 (2005).
 [39] M. Fuchs and M. Scheffler, *Comput. Phys. Commun.* **119**, 67 (1999).
 [40] N. Troullier and J. L. Martins, *Phys. Rev. B* **43**, 1993 (1991).
 [41] H. J. Monkhorst and J. D. Pack, *Phys. Rev. B* **13**, 5188 (1976).
 [42] M. D. Pashley, *Phys. Rev. B* **40**, 10481 (1989).
 [43] M. Bernasconi, G. L. Chiarotti, and E. Tosatti, *Phys. Rev. B* **52**, 9988 (1995).
 [44] Y. Takao and A. Morita, *Physica B* **105**, 93 (1981).
 [45] V. Kumar and B. S. R. Sastry, *Phys. Status Solidi B* **242**, 869 (2005).
 [46] P. Lautenschlager, M. Garriga, L. Vina, and M. Cardona, *Phys. Rev. B* **36**, 4821 (1987).
 [47] S. Zollner, M. Garriga, J. Kircher, J. Humlíček, M. Cardona, and G. Neuhold, *Thin Solid Films* **233**, 185 (1993).
 [48] O. Supplie, T. Hannappel, M. Pristovsek, and H. Döscher, *Phys. Rev. B* **86**, 035308 (2012).
 [49] I. Németh, B. Kunert, W. Stolz, and K. Volz, *J. Cryst. Growth* **310**, 1595 (2008).
 [50] M. Kondo, C. Anayama, N. Okada, H. Sekiguchi, K. Domen, and T. Tanahashi, *J. Appl. Phys.* **76**, 914 (1994).
 [51] S. L. Wright, M. Inada, and H. Kroemer, *J. Vac. Sci. Technol.* **21**, 534 (1982).
 [52] R. Bringans, *Crit. Rev. Solid State* **17**, 353 (1992).
 [53] S. M. Ting and E. A. Fitzgerald, *J. Appl. Phys.* **87**, 2618 (2000).
 [54] R. D. Bringans, D. K. Biegelsen, and L.-E. Swartz, *Phys. Rev. B* **44**, 3054 (1991).
 [55] G. Steinbach, M. Schreiber, and S. Gemming, *Nanosci. Nanotechnol. Lett.* **5**, 73 (2013).
 [56] S. L. Wright, H. Kroemer, and M. Inada, *J. Appl. Phys.* **55**, 2916 (1984).